Reaction Kinetics, Mechanisms and Catalysis
https://doi.org/10.1007/s11144-024-02713-y

Oxidation of hydrogen peroxide by tungstate ion: formation and decay of a long-lived intermediate

Joaquin F. Perez-Benito[1] · **Adria Salido-Pons**[1]

Received: 7 July 2024 / Accepted: 12 August 2024

Abstract

The kinetics of the reaction between tungstate ion and hydrogen peroxide in aqueous medium containing phosphate ions has been followed spectrophotometrically at 225 nm. This wavelength led to two different kinds of absorbance-time plots, showing either an increasing-maximum-decreasing temporal pattern or a continuously decreasing one, depending on the medium pH. This allowed to carry out two independent kinetic studies, one at high pH (first reaction stage) concerning the formation of a long-lived intermediate, thought to be W(V), and the other at low pH (second reaction stage) concerning its decay. The kinetic tool chosen to obtain the quantitative information was that of the initial rate method. The results indicated that, whereas both reaction stages were of first order in hydrogen peroxide, the rate dependence on the concentration of tungstate ion differed for the two stages: an apparent kinetic order intermediary between 1 and 2 for the first stage, and a well-defined order 1 for the second stage. There was also a difference between the dependences of the initial rates of the two stages on the concentrations of phosphate ions (the rate of the first stage independent and that of the second decreasing) and of the background electrolyte KCl (for the first stage an increasing effect and for the second a decreasing one). Both stages showed catalysis by hydrogen, copper(II), zinc and manganese(II) ions, the latter three probably acting as superoxide radical scavengers. Although the activation energy of the first stage was unusually close to zero (1.0 ± 1.2 kJ mol^{-1}), that of the second stage was considerably higher (28 ± 3 kJ mol^{-1}). Finally, a mechanism coherent with the available experimental information, and where the solvent cage effect plays an important role, has been proposed for each reaction stage.

✉ Joaquin F. Perez-Benito
jfperezdebenito@ub.edu

[1] Departamento de Ciencia de Materiales y Quimica Fisica, Seccion de Quimica Fisica, Facultad de Quimica, Universidad de Barcelona, Marti i Franques 1, 08028 Barcelona, Spain

Published online: 29 August 2024

Graphical abstract

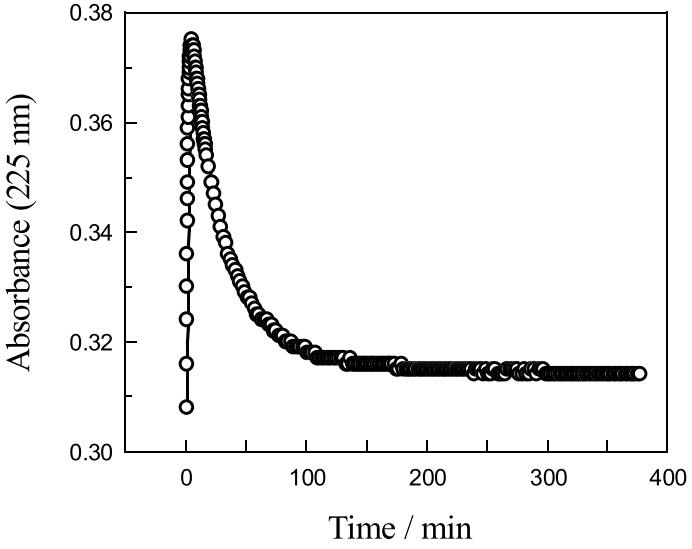

Keywords Catalysis · Hydrogen peroxide · Kinetic study · Mechanism · Solvent cage effect · Tungstate ion

Introduction

Tungsten is one of the four elements belonging to the VIB group of the periodic table, the only others of some importance in the chemistry laboratory being chromium and molybdenum [1]. With respect to the chemical properties, those of the VI oxidation state are remarkable. For instance, both molybdenum(VI) and tungsten(VI) have been reported to catalyze the oxidation of organic compounds by hydrogen peroxide [2]. Although the elements with an atomic number $Z > 35$ are known not to have usually a biological role in healthy leaving organisms, tungsten with its $Z = 74$ is an exception because of its active participation in the constitution of several enzymes [3].

On its part, hydrogen peroxide is a versatile reagent, acting either as an oxidizing agent [4–6] or as a reducing one [7–9], depending on its chemical counterpart. It can even dismutate in the presence of an adequate catalyst [10–12]. With respect to the biological properties, this peroxide is one of the metabolites formed in the cell's mitochondria of aerobes after the oxygen uptake [13–15]. Its main harmful effects are probably related to its ability to generate free radicals by reaction with transition metal ions (or their protein complexes) readily susceptible of accepting or donating one electron in redox processes, yielding superoxide radicals in the first case [16–18] and hydroxyl radicals in the second [19–21]. Since those reactive oxygen species (ROS) are believed to be involved in the mechanism of aging [22–24], as well as in the genesis of some

types of cancer [25–27] and other degenerative diseases 28–30], the organism is prepared to defend itself from them by eliminating their chemical source. To this purpose, the enzymes catalase and glutathione peroxidase catalyze the efficient dismutation of hydrogen peroxide (leading to H_2O and O_2) [31–33] and its reduction to water [34–36], respectively.

Since it is clear that those natural enzymes do not seem to be able to completely avoid the generation of free radicals, and so arresting what might be the main route of the aging process, it may be interesting to look for low-toxicity chemical species capable of eliminating hydrogen peroxide (by either its oxidation to O_2 or its reduction to H_2O), ideally in two-electron reactions, that is, without the mediation of deleterious free radicals in the corresponding mechanism. In this work, and with that perspective in mind, the oxidation of hydrogen peroxide to diatomic oxygen by tungstate ion will be analyzed in detail. Besides the oxidation reaction, there might also be some catalysis of the decomposition of hydrogen peroxide, contributing to some extent to the overall reaction. Actually, chromate ion has been reported to oxidize hydrogen peroxide under acidic conditions (it being reduced to the + III state), whereas what happens in neutral solutions is the catalysis of the decomposition of the peroxide:

$$2H_2O_2 \longrightarrow 2H_2O + O_2 \tag{1}$$

the catalyst being recuperated at the end of the reaction [37]. A similar behavior might be expected to be found a priori in the case of tungstate ion.

Experimental

Materials

The solvent used in all the experiments was water previously purified by deionization followed by treatment with a Millipore Synergy UV system (milli-Q quality, $K = 0.05$ μS/cm at 25.0 °C). The three reactants required to carry out the redox reaction and thus present in all the kinetic runs were sodium tungstate dihydrate, $Na_2WO_4{\cdot}2H_2O$ (Fluka), as the oxidizing agent; hydrogen peroxide, H_2O_2 (Sigma-Aldrich), as the reducing agent; and potassium dihydrogen phosphate, KH_2PO_4 (Merck), as the acid component of a buffer. Moreover, the chemical compounds present in some of the experiments were hydrochloric acid, HCl (Sigma-Aldrich), and sodium hydroxide, NaOH (Panreac), to change the pH of the medium when necessary; potassium chloride, KCl (Merck), to change the ionic strength; as well as copper(II) sulfate pentahydrate, $CuSO_4{\cdot}5H_2O$ (Merck), zinc sulfate heptahydrate, $ZnSO_4{\cdot}7H_2O$ (Merck), and manganese(II) sulfate monohydrate, $MnSO_4{\cdot}H_2O$ (Merck), as potential catalysts.

Instrumentation

The pH measurements were done by means of a Wave pH-meter, provided with a digital presentation until the second decimal figure (± 0.01 pH) and an anode–cathode electrode pair, the latter calibrated with the aid of commercial buffers of known

pH. The temperature was kept constant by means of a thermostatic bath Lauda E 100 also provided with a digital reading (± 0.1 °C). Given that the reacting mixtures were all colorless, the kinetic runs were followed measuring periodically the absorbances at 225 nm with a Shimadzu 160 A double beam UV–Vis spectrophotometer (± 0.001 *A*), with a thermostatted cell holder and using a quartz cell of 1 cm optical path length. That wavelength offers two advantages, the first one being that it allows to determine the initial rate of formation of a long-lived intermediate at higher pHs and of the reaction products at lower pHs; the second one being that it leads to large increases or decreases in the solution absorbance, thus minimizing the experimental errors associated with the determination of the kinetic parameters.

Kinetic experiments

The oxidizing agent, sodium tungstate, was the last reactant to be added to a thermostatted aqueous solution containing all the other required chemicals. The total volume of the reaction mixtures was fixed at a constant value (24 mL) in all the experiments. The absorbance readings started around 20–25 s after the last reactant was added (usually by means of a fast release 1-mL pipette) and the reaction mixture gently stirred. The absorbances were then periodically measured, in the first stage of the process, when the reaction was rather fast, with a time interval of 10 s during 16 min (99 values), and in the last stage, already at a lower rate as the reaction nears the equilibrium, with a time interval of 120 s during several hours. In total, 279 kinetic runs were performed.

Results and discussion

Experimental absorbance-time plots

In the first experiment, the reaction was followed simultaneously at five different wavelengths, covering almost the whole ultraviolet spectrum range. This was so because the reacting mixture was colorless throughout the reaction, thus rendering useless the visible part of the spectrum. The wavelength of 225 nm was clearly the one leading to a wider change in the absorbance (in this case a decrease) as the reaction advanced, and so it was selected to monitor the evolution of the process (Fig. 1S, left).

A striking finding of this experiment was that the profile of each absorbance-time plot depended a lot on the wavelength of work. At both 225 nm (Fig. 1S, right) and 250 nm (Fig. 2S, left) the absorbance monotonously decreased with time, at 275 nm it increased throughout the reaction (Fig. 2S, right), whereas at both 300 nm (Fig. 3S, left) and 325 nm (Fig. 3S, right) the absorbance presented a maximum, with a fast increase followed by a slow decrease. When the absorbance vs. time plot showed a monotonously decreasing profile (225 and 250 nm), the chemical species responsible for that decrease was either a reactant or a long-lived intermediate after its maximum concentration. The continuously increasing

profile (275 nm) seemed to be the result of a reaction product absorbing light at that wavelength. Finally, the plots showing a maximum (300 and 325 nm) were indeed caused by a long-lived intermediate (I-1), most probably the same at both wavelengths, but with a molar absorption coefficient higher at the lower one ($\varepsilon_{300} > \varepsilon_{325}$). However, the increase in absorbance associated with the formation of I-1 was too low for allowing the determination of kinetic parameters with a reasonable precision.

Working from now on at the selected wavelength of 225 nm, the tungstate-hydrogen peroxide reaction presented a rather unique feature, since the profiles of the absorbance vs. time plots dramatically changed with the pH of the medium. Whereas at high pHs the plots showed an initial increasing stage followed by a maximum and a decreasing one (Fig. 1, left), what we observed at low pHs was a monotonously decreasing stretch, sometimes (especially when the concentration of phosphate ions was very low) followed by an increasing one (Fig. 1, right).

The first kind of behavior (plot with a maximum) clearly indicated that another long-lived intermediate (I-2), absorbing light at 225 nm, was being formed. Although there was little information on the nature of these two long-lived intermediates, a reasonable guess would be that I-2 might be a W(V) species, whereas I-1 might be a superoxotungsten(III) species (WOO^{2+}), by analogy with superoxochromium(III) ion ($CrOO^{2+}$) [38, 39], whose electronic spectrum shows an absorption peak at 290 nm, and which has been reported to be formed from the reaction of Cr(IV) with H_2O_2 [40]. These two intermediates had to be present in concentration high enough for the spectrophotometer to be able to detect them, and thus not being in steady state, since this approximation would require that the intermediates be reactive enough for their maximum concentrations to be negligible with respect to the initial concentration of the limiting reactant (tungstate ion) [41].

On its side, the second kind of behavior (plot without a maximum and at low pH) might correspond to a situation where the long-lived intermediate I-2 had already been formed when the first absorbance reading was taken, suggesting that the conversion of the reactants into that intermediate exhibited acid catalysis.

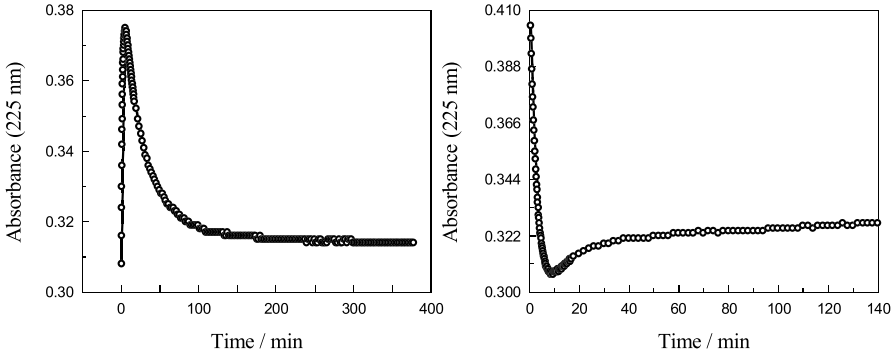

Fig. 1 Absorbance at 225 nm as a function of time during the tungstate ion-hydrogen peroxide reaction at $[Na_2WO_4]_o = 2.67 \times 10^{-4}$ M, $[H_2O_2]_o = 1.63 \times 10^{-3}$ M and 25.0 °C. Left: $[KH_2PO_4]_o = 1.50 \times 10^{-2}$ M, $[NaOH]_o = 2.46 \times 10^{-3}$ M and pH 6.12. Right: $[KH_2PO_4]_o = 3.00 \times 10^{-3}$ M, $[NaOH]_o = 0$ and pH 5.74

Initial rate method

Given the complexity of the tungstate ion-hydrogen peroxide reaction, the initial rate method was the one chosen to obtain the kinetic data. This method was splitted into two different versions, depending on whether we referred to the formation of the long-lived intermediate (from now on I-2) from the reactants (absorbance increasing with time):

$$\ln (A_{\infty} - A_t) = a_o + a_1 t + a_2 t^2 \tag{2}$$

or to that of the reaction products from the intermediate (absorbance decreasing with time):

$$\ln (A_t - A_{\infty}) = a_o + a_1 t + a_2 t^2 \tag{3}$$

the fit being limited to the first 10 experimental points (90 s), whereas the formula used in both cases to obtain the initial rate was:

$$v_o = - \left(\frac{d[\mathrm{W(VI)}]_t}{dt} \right)_{t=0} = - a_1 [\mathrm{W(VI)}]_o \tag{4}$$

the relationship between absorbances and concentrations having been based on the known equation for additive properties [42].

Main kinetic data

An increase in the initial concentration of tungstate ion, keeping all the other experimental conditions constant, led to linear relationships in double-logarithmic plots of the initial rate against that concentration, both as far as the formation of the long-lived intermediate (Fig. 4S, left) and its posterior decay (Fig. 4S, right) were concerned. The two slopes were positive but non-integer numbers, 1.70 ± 0.05 in the first case and 0.63 ± 0.03 in the second. However, since sodium tungstate is a basic compound, the medium pH increased as its concentration increased, pointing out that a correction of these results will be required later.

When the effect of the reducing agent on the reaction rate was studied, the double-logarithmic plots also led to linear relationships, yielding this time kinetic orders for hydrogen peroxide very close to unity, 0.99 ± 0.03 as far as the formation of the intermediate is concerned (Fig. 5S, left) and 1.00 ± 0.02 for its decay (Fig. 5S, right).

The initial rate corresponding to the formation of the long-lived intermediate increased with the potassium dihydrogen phosphate concentration showing an upward-concave curvature (Fig. 2, left), whereas that corresponding to the intermediate decay showed a maximum and a bell-shaped profile (Fig. 2, right). The simplest explanation for these behaviors would be that both stages of the reaction presented acid catalysis, since an increase of the KH_2PO_4 concentration resulted in a decrease in the medium pH, but the second stage also showed an inhibition by phosphate ions, the latter being responsible for the decrease observed in the rate value. Actually, phosphate ions are known to form stable complexes with both Mo(VI)

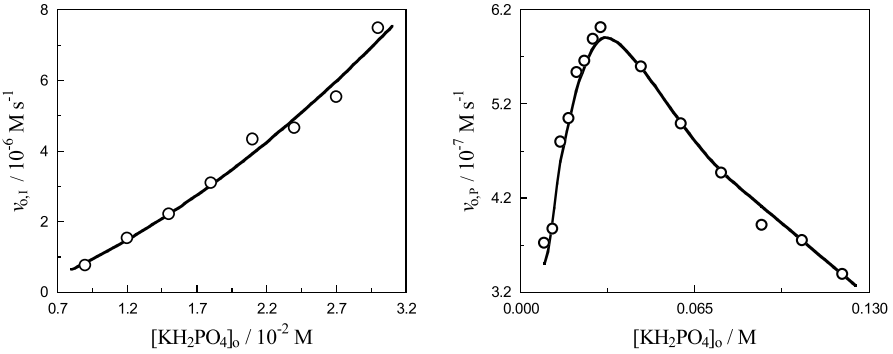

Fig. 2 Initial rate as a function of the potassium dihydrogen phosphate initial concentration at $[Na_2WO_4]_o = 2.67 \times 10^{-4}$ M, $[H_2O_2]_o = 1.63 \times 10^{-3}$ M and 25.0 °C. Left: formation of the long-lived reaction intermediate at $[KH_2PO_4]_o = 9.00 \times 10^{-3}$ M (pH 6.54)–3.00×10^{-2} M (pH 5.92) and $[NaOH]_o = 3.40 \times 10^{-3}$ M. Right: formation of the reaction products at $[KH_2PO_4]_o = 9.00 \times 10^{-3}$ M (pH 5.33)–0.120 M (pH 4.52) and $[NaOH]_o = 0$

[43–45] and W(VI) [46–48], thus offering a possible explanation for the observed inhibition by those ions.

The potential effect induced by the medium ionic strength on the reaction rate was studied by making use of potassium chloride as background electrolyte. Rather surprisingly, the observed behaviors for the two reaction stages were opposite of each other, whereas the initial rate of intermediate formation increased as the KCl initial concentration increased (Fig. 3, left), that of its decay decreased (Fig. 3, right). Addition of KCl resulted in a decrease of the medium pH, caused by its effect on the dissociation equilibrium of dihydrogen phosphate ion, shifting it to the right (an ionic strength effect). Since both reaction stages seemed to show acid catalysis, the actual effects of the ionic strength on the rate (once discounted the pH effect) were expected to be less intense than that observed in the laboratory for the first stage and more intense for the second.

The effect of the pH on the reaction rate, although partially guessed from the results found when the KH_2PO_4 initial concentration was changed (Figs. 2, left and right), was studied in more detail by changing this time the concentrations of HCl and NaOH as necessary, so that the masking effect caused by a potential phosphate-induced inhibition could be avoided. Acid catalysis was found for both the formation of the long-lived intermediate (Fig. 4, left) and its decay (Fig. 4, right). Interestingly enough, the plot observed in the second case was monotonously decreasing, thus demonstrating that the maximum observed in Fig. 2 (right) was caused by a combination of acid catalysis and inhibition by phosphate ions. However, a comparison of the curves corresponding to the initial rate of formation of the long-lived intermediate at different pHs obtained at constant (with addition of NaOH) and variable phosphate concentrations (Fig. 6S) showed that only the decay of the long-lived intermediate was affected by the presence of phosphate ions, the formation of that intermediate being largely unaffected. The experimental data for the first (Table 1) and second (Table 2) reaction stages could be fitted to the following equations:

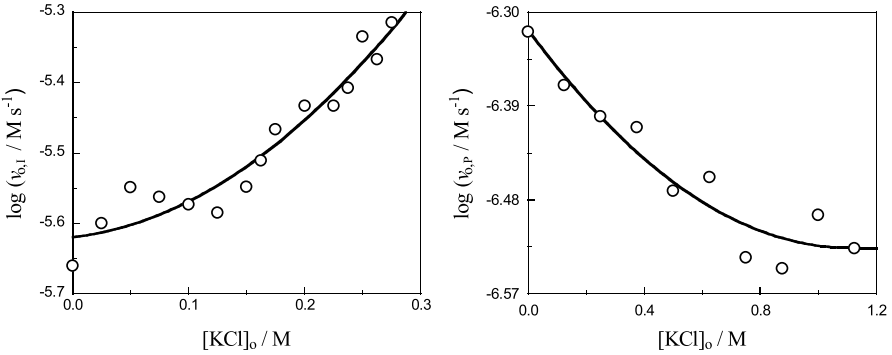

Fig. 3 Logarithm of the initial rate as a function of the potassium chloride initial concentration at $[Na_2WO_4]_o = 2.67 \times 10^{-4}$ M, $[H_2O_2]_o = 1.63 \times 10^{-3}$ M, $[KH_2PO_4]_o = 1.50 \times 10^{-2}$ M and 25.0 °C. Left: formation of the long-lived reaction intermediate at $[NaOH]_o = 3.40 \times 10^{-3}$ M and $[KCl]_o = 0$ (pH 6.29)–0.275 M (pH 6.16). Right: formation of the reaction products at $[NaOH]_o = 0$ and $[KCl]_o = 0$ (pH 5.09)–1.125 M (pH 4.95)

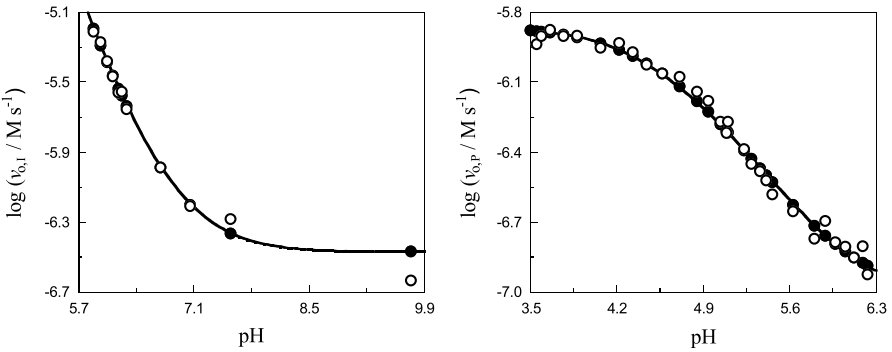

Fig. 4 Logarithm of the initial rate as a function of the pH at $[Na_2WO_4]_o = 2.67 \times 10^{-4}$ M, $[H_2O_2]_o = 1.63 \times 10^{-3}$ M, $[KH_2PO_4]_o = 1.50 \times 10^{-2}$ M and 25.0 °C, showing both the experimental points (empty circles) and those calculated according to a theoretical model (filled circles). Left: formation of the long-lived reaction intermediate at $[HCl]_o = 0$ and $[NaOH]_o = 1.41 \times 10^{-3}$ M–1.76×10^{-2} M, the model being given by Eq. 5. Right: formation of the reaction products at $[HCl]_o = 0$–1.01×10^{-3} M (pH ≤ 5.09) and $[NaOH]_o = 0$–3.17×10^{-3} M (pH ≥ 5.09), the model being given by Eq. 6

$$v_{o,I} = k_{H,1} + k_{H,2}\,[H^+] + k_{H,3}\,[H^+]^2 \tag{5}$$

$$v_{o,P} = \frac{k_{H,4} + k_{H,5}\,[H^+]}{1 + k_{H,6}\,[H^+]} \tag{6}$$

The formation of the long-lived intermediate was essentially non-dependent on temperature, the activation energy being close to zero (1.0 ± 1.2 kJ mol^{-1}) and, accordingly, with the correlation coefficient associated with the Arrhenius plot

Table 1 pH-Related kinetic parameters associated with the formation of the long-lived reaction intermediate[a]

Parameter[b]	Numerical value	Units
$k_{H,1}$	$(3.4 \pm 0.7) \times 10^{-7}$	Ms^{-1}
$k_{H,2}$	3.22 ± 0.11	s^{-1}
$k_{H,3}$	$(1.1 \pm 0.2) \times 10^{6}$	$M^{-1}\ s^{-1}$

[a]$[Na_2WO_4]_o = 2.67 \times 10^{-4}$ M, $[H_2O_2]_o = 1.63 \times 10^{-3}$ M, $[KH_2PO_4]_o = 1.50 \times 10^{-2}$ M, $[NaOH]_o = 1.41 \times 10^{-3}$ M–1.76×10^{-2} M, pH 5.89–9.74, 25.0 °C

[b]Parameters defined in Eq. 5

Table 2 pH-Related kinetic parameters associated with the decay of the long-lived reaction intermediate[a]

Parameter[b]	Numerical value	Units
$k_{H,4}$	$(8.9 \pm 0.5) \times 10^{-8}$	Ms^{-1}
$k_{H,5}$	$(7.52 \pm 0.09) \times 10^{-2}$	s^{-1}
$k_{H,6}$	$(5.4 \pm 0.4) \times 10^{4}$	M^{-1}

[a]$[Na_2WO_4]_o = 2.67 \times 10^{-4}$ M, $[H_2O_2]_o = 1.63 \times 10^{-3}$ M, $[KH_2PO_4]_o = 1.50 \times 10^{-2}$ M, $[HCl]_o = 0$–1.01×10^{-3} M (pH ≤ 5.09), $[NaOH]_o = 0$–3.17×10^{-3} M (pH ≥ 5.09), 25.0 °C

[b]Parameters defined in Eq. 6

Table 3 Kinetic parameters for the tungstate-hydrogen peroxide reaction

Parameter	Intermediate formation	Product formation
Kinetic order (WO_4^{2-})[a]	1.70 ± 0.05	0.63 ± 0.03
Kinetic order (WO_4^{2-})[b]	1.85 ± 0.04	1.01 ± 0.06
Kinetic order (H_2O_2)	0.99 ± 0.03	1.00 ± 0.02
Activation energy	1.0 ± 1.2 kJ mol^{-1}	28 ± 3 kJ mol^{-1}

[a]Non-corrected values

[b]pH-corrected values

rather low (Fig. 7S, left). The activation energy for the intermediate decay was considerably higher (28 ± 3 kJ mol^{-1}) and with a more acceptable correlation coefficient (Fig. 7S, right).

A compilation of the main kinetic results obtained for the tungstate ion-hydrogen peroxide reaction can be found in Table 3. As can be seen, when the effect of the changing pH due to the basicity of the oxidizing agent (Na_2WO_4) was discounted, the kinetic order of that species increased from 1.70 to 1.85 in the case of the intermediate formation and from 0.63 to 1.01 in that of its decay. The kinetic order of hydrogen peroxide, however, did not require any correction, since the corresponding series of experiments was carried out at almost constant pH. It should also be noticed the striking difference in the activation energies observed for the two reaction stages.

Catalysis by transition metal ions

The eventual possibility of catalysis by transition metal ions was also addressed. In particular, copper(II) and zinc ions are known to be involved in the composition of the mitochondrial superoxide dismutase enzyme (Cu,Zn-SOD) [49, 50], whereas manganese(II) ion is involved in that of cytoplasmic superoxide dismutase (Mn-SOD) [51–53]. Thus, it might be interesting to study the effect of those ions on the reaction rate, since most electrophilic agents are known to oxidize hydrogen peroxide to the superoxide ion radical in the first elementary step of the mechanism [54–56].

Starting with copper(II) ion, we found the existence of catalysis for both the formation of the long-lived intermediate (Fig. 5, left) and its decay (Fig. 5, right), but showing a very different kind of behavior. As far as the intermediate formation was concerned, the initial period of catalysis by Cu(II) was followed by another of apparent saturation (horizontal stretch), whereas at higher concentrations of that metal ion the precipitation of a white solid was observed, suggesting that the horizontal stretch found at lower concentrations was caused by the formation of a phosphate-copper(II) soluble colloid. Thus, a further increase in the Cu(II) concentration resulted in an increase in the size and number of colloidal particles, instead of remaining free in the solution to act as catalyst. That soluble colloid might also explain the anomalous behavior reported for the copper(II) ion-hydrogen peroxide reaction in the presence of a phosphate buffer [10], although in that case the colloidal particles seemed to show some catalytic activity on that reaction. The effect of copper(II) ion on the initial rate for the conversion of the long-lived intermediate into the reaction products was indeed much simpler, leading to a first-order dependence on the catalyst concentration. The finding that at these lower pHs (5.07–5.20) no formation of either a soluble colloid or a precipitate was observed, whereas at a higher pH (6.26) both of them where observed, seemed to indicate that the insoluble chemical species was $CuHPO_4$ instead of $Cu(H_2PO_4)_2$.

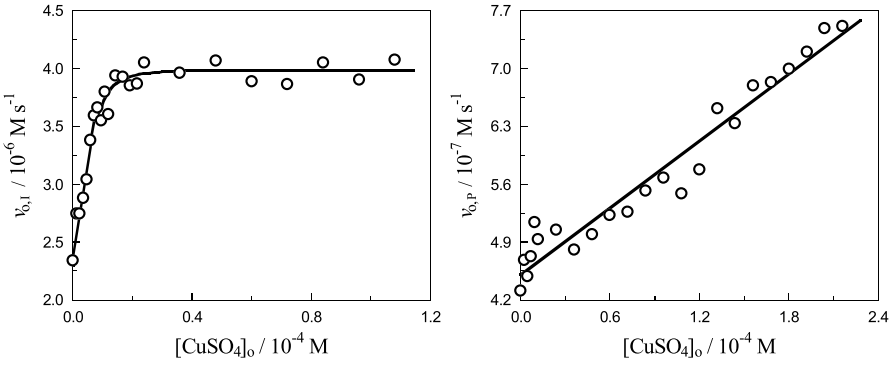

Fig. 5 Initial rate as a function of the copper(II) sulfate initial concentration at $[Na_2WO_4]_o = 2.67 \times 10^{-4}$ M, $[H_2O_2]_o = 1.63 \times 10^{-3}$ M, $[KH_2PO_4]_o = 1.50 \times 10^{-2}$ M and 25.0 °C. Left: formation of the long-lived reaction intermediate at $[NaOH]_o = 3.40 \times 10^{-3}$ M and pH 6.26 ± 0.01. Right: formation of the reaction products at $[NaOH]_o = 0$ and $[CuSO_4]_o = 0$ (pH 5.20)–2.16×10^{-4} M (pH 5.07), with $r = 0.975$

In the case of zinc ion, catalysis was again observed in both reaction stages, for the accumulation of the long-lived intermediate (Fig. 8S, left) and for its decay (Fig. 8S, right). However, the saturation limit evidencing the formation of a soluble colloid was now present not only at high values of the medium pH but also at low values. In addition, a white precipitate (most likely, $ZnHPO_4$) was observed at high pH when the concentration of zinc ion was high enough.

On its hand, in the case of manganese(II) ion, catalysis was observed in both reaction stages, for the accumulation of the long-lived intermediate (Fig. 9S, left) and for its decay (Fig. 9S, right). However, in the first reaction stage (formation of the intermediate) the catalysis was followed by some inhibition at higher concentrations of manganese(II), suggesting that this metal ion might act as a reductant of the long-lived intermediate. The high dispersion of the experimental points in both figures might be caused by the formation of a soluble form of colloidal manganese dioxide as another long-lived intermediate [57].

UV spectra at the end of the reaction

The final UV spectra corresponding to the reaction products (recorded 24 h later), showed a shoulder at high pH, but that turned out into an absorption peak at 250 nm when the medium pH was low enough. This finding suggests that the final electronic spectra were caused by at least two different chemical species, the one responsible for the peak likely being tungsten with a lower oxidation state than the other, given that the reducibility of the transition metal oxyanions is known to increase by protonation [58]. The same behavior was observed at higher pHs, but only in the presence of divalent transition metal ions, either Zn^{2+}, Cu^{2+} or Mn^{2+}. The wavelength at which appears the absorbance peak suggests that the responsible species might be a cationic transition metal complex with a superoxide ion ligand (WO_2^{2+}, ZnO_2^{+}, CuO_2^{+} or MnO_2^{+}) [59, 60].

Formation of the long-lived intermediate: mechanism and rate law

In order to explain the experimental results, we have proposed for the first (absorbance-increasing) reaction stage a mechanism that starts with four fast reversible (quasi-equilibrium) steps, followed by other four slow (rate-determining) steps belonging each one of them to a different reaction pathway, and ending with two fast (non-rate-determining) steps:

$$W^{VI}O_4^{2-} + H^+ \overset{K_1}{\leftrightharpoons} HW^{VI}O_4^- \tag{7}$$

$$W^{VI}O_4^{2-} + H_2O_2 \overset{K_2}{\leftrightharpoons} [W^{VI}O_3(O_2)]^{2-} + H_2O \tag{8}$$

$$HW^{VI}O_4^- + H_2O_2 \overset{K_3}{\leftrightharpoons} H[W^{VI}O_3(O_2)]^- + H_2O \tag{9}$$

$$H\,[W^{VI}O_3(O_2)]^- \overset{K_4}{\leftrightarrows} [W^{V}O_3^- + HO_2^{\bullet}]_{sc} \tag{10}$$

$$[W^{VI}O_3(O_2)]^{2-} \xrightarrow[\text{slow}]{k_5} W^{V}O_3^- + O_2^{\bullet -} \tag{11}$$

$$[W^{V}O_3^- + HO_2^{\bullet}]_{sc} \xrightarrow[\text{slow}]{k_6} W^{V}O_3^- + HO_2^{\bullet} \tag{12}$$

$$[W^{V}O_3^- + HO_2^{\bullet}]_{sc} + W^{VI}O_4^{2-} \xrightarrow[\text{slow}]{k_7} 2W^{V}O_3^- + O_2 + HO^- \tag{13}$$

$$[W^{V}O_3^- + HO_2^{\bullet}]_{sc} + HW^{VI}O_4^- \xrightarrow[\text{slow}]{k_8} 2W^{V}O_3^- + O_2 + H_2O \tag{14}$$

$$HO_2^{\bullet} + O_2^{\bullet -} \rightarrow HO_2^- + O_2 \tag{15}$$

$$HO_2^- + H_2O \leftrightarrows H_2O_2 + HO^- \tag{16}$$

It is generally accepted that, as far as redox reactions are concerned, the finding of acid catalysis usually means that protonation of the oxidant takes place before the rate-determining step, resulting in a decrease in its electron density and so in an enhancement of its electron affinity, whereas the existence of base catalysis means that deprotonation of the reducing agent is happening, resulting in an increase in its electron density and so in an enhancement of its electron donating capacity.

Consequently, our mechanism begins with the protonation of the oxidant, tungstate ion, in Eq. 7 to account for the observed acid catalysis. In the following steps hydrogen peroxide reacts with both tungstate (Eq. 8) and hydrogen tungstate (Eq. 9) ions to form monoperoxo complexes. The transition metals of the VIB group in their highest oxidation state are actually known to form stable peroxo complexes: peroxochromate(VI) [61, 62], peroxomolybdate(VI) [63–65] and peroxotungstate(VI) [66, 67] ions.

Once formed the peroxo complexes, the occurrence of an internal redox process leads to the formation of W(V) and either the protonated form of superoxide radical (forward direction in Eq. 10) or its non-protonated form (Eq. 11), but, whereas the first of these two reactions has been proposed as a reversible step, the second has been proposed as an irreversible one. The reason for this divergence is double: in the first case an anion and a neutral molecule are formed, with a clear tendency to become trapped in the same cage of solvent, whilst in the second case two anions are formed, so that their mutual electrostatic repulsion will facilitate their escape from the solvent cage; moreover, the protonated (neutral) form of superoxide radical possesses a lower electron density than its free (anionic) form, and so a higher electron affinity, thus being able to reoxidize W(V) to W(VI) (backward direction in Eq. 10).

Since the two species generated as reaction products in Eq. 10 are formed together, the solvent cage effect allows us to treat the couple as a single

species [68–70]. Although more often than not the couple will regenerate the peroxotungstate(VI) complex, once in a while the two intermediates locked in the solvent cage could have three possible fates: escaping from the solvent cage (Eq. 12), or else react with either tungstate ion (Eq. 13) or its protonated form (Eq. 14). Hence, according to the proposed mechanism, the long-lived intermediate W(V) is formed in four different rate-determining steps (Eqs. 11–14).

In the first of the final two non-rate-determining steps, the well-known dismutation of the superoxide radicals takes place (Eq. 15), the low electron-density protonated form acting as oxidant and the high electron-density free form acting as reductant [71]. Protonation of the hydroperoxide ion formed in that step by abstraction of a hydrogen atom from a water molecule leads to regeneration of the reducing agent (Eq. 16).

The rate can be defined as the time derivative of the tungsten(V) concentration, since this species has been postulated to be the long-lived intermediate formed in the first reaction stage. By application of the quasi-equilibrium approximation to Eqs. 7–10, we arrive at:

$$\frac{d\,[\mathrm{W(V)}]}{d\,t} = (K_2\,k_5 + K_1\,K_3\,K_4\,k_6\,[\mathrm{H^+}] + f\,)\,[\mathrm{WO_4^{2-}}]\,[\mathrm{H_2O_2}] \tag{17}$$

In this equation:

$$f = 2K_1\,K_3\,K_4(k_7 + K_1\,k_8\,[\mathrm{H^+}])\,[\mathrm{WO_4^{2-}}]\,[\mathrm{H^+}] \tag{18}$$

Equations 17 and 18 can explain the experimental results found for the formation of the long-lived intermediate: apparent kinetic order between 1 and 2 for tungstate ion, order 1 for hydrogen peroxide, and catalysis by hydrogen ion. The dependence on the concentration of the latter is coherent with Eq. 5 with:

$$k_{\mathrm{H},1} = K_2\,k_5\,[\mathrm{WO_4^{2-}}]\,[\mathrm{H_2O_2}] \tag{19}$$

$$k_{\mathrm{H},2} = K_1\,K_3\,K_4(k_6 + 2k_7\,[\mathrm{WO_4^{2-}}])\,[\mathrm{WO_4^{2-}}]\,[\mathrm{H_2O_2}] \tag{20}$$

$$k_{\mathrm{H},3} = 2K_1^2K_3\,K_4\,k_8\,[\mathrm{WO_4^{2-}}]^2\,[\mathrm{H_2O_2}] \tag{21}$$

According to these results, of the four rate-determining steps proposed in this part of the mechanism it is that associated with rate constant k_7 (Eq. 13), corresponding to the partial kinetic orders 1 in hydrogen ion and 2 in tungstate ion, the one responsible for the greatest contribution to the total reaction rate.

Moreover, the rate increasing effect of the medium ionic strength when KCl was used as background electrolyte is consistent with the associated increase in rate constants k_7 and k_8, since both Eqs. 13 and 14 imply the bimolecular reaction between two anions, whereas the unusual finding of an activation energy close to zero could be explained provided the quasi-equilibria depicted in Eqs. 8 and 9 are exothermic enough (ΔH_2°, $\Delta H_3^{\circ} < < 0$).

Although the finding of a higher than one apparent order in W(VI) has been conveniently explained by Eqs. 13 and 14, it should be pointed out that an alternative explanation is possible. In fact, both molybdate and tungstate ions are known to polymerize in acid solution [72], and it has been reported that hydrogen peroxide complexes both Mo(VI) and W(VI) polymers [73]. Moreover, phosphate-tungstate polyoxometalates have been reported, although aggregation does not occur in highly diluted solutions [74]. Therefore, even if the range of concentrations of W(VI) employed in this study was rather low, the unusual kinetic order found here for tungstate ion might be at least partially related to that polymerization.

A concentration of copper(II) ion as small as two orders of magnitude lower than that of the limiting reactant (tungstate ion) had an observable catalytic effect on the reaction rate. This finding suggests that the catalyst is reacting with a very dilute reaction intermediate. When that transition metal ion is present as catalyst, the following reactions are very likely involved in the mechanism:

$$[W^{V}O_3^- + HO_2^{\bullet}]_{sc} + Cu^{2+} \xrightarrow[\text{slow}]{k_9} W^{V}O_3^- + O_2 + Cu^{+} + H^{+} \tag{22}$$

$$Cu^{+} + W^{VI}O_4^{2-} + H_2O \longrightarrow Cu^{2+} + W^{V}O_3^- + 2HO^- \tag{23}$$

Actually, both free copper(II) ion [71] as well as some of its complexes [75] are known to oxidize superoxide radicals, thus showing some SOD mimetic activity. The new intermediate formed, copper(I) ion, is known to be a strong reducing agent [76], thus capable of reacting with W(VI) in Eq. 23 to yield once again the long-lived intermediate W(V).

Now, considering that copper(I) ion is reactive enough to be in steady state, what is indeed consistent with its well-known exacerbated reducing power, the total reaction rate will be:

$$\frac{d\,[\mathrm{W(V)}]}{d\,t} = v_{nc} + 2K_1\,K_3\,K_4\,k_9\,[WO_4^{2-}]\,[H_2O_2]\,[H^{+}]\,[Cu^{2+}] \tag{24}$$

Here v_{nc} is the rate of the non-catalytic reaction pathway, given by Eqs. 17 and 18.

In the case of the two other transition metal ions acting as catalysts for the tungstate ion-hydrogen peroxide reaction, zinc and manganese(II) ions, since their reduction to a lower oxidation state by the superoxide ion radical would be rather unlikely, we can propose instead:

$$[W^{V}O_3^- + HO_2^{\bullet}]_{sc} + M^{2+} \xrightarrow[\text{slow}]{k_{10}} W^{V}O_3^- + MO_2^{+} + H^{+} \tag{25}$$

$$MO_2^{+} + W^{VI}O_4^{2-} + H_2O \longrightarrow M^{2+} + W^{V}O_3^- + O_2 + 2HO^- \tag{26}$$

Here M stands for either Zn or Mn and, by application of the steady state approximation to the short-lived intermediate MO_2^{+}, a rate law formally analogous to Eq. 24 would be obtained.

Decay of the long-lived intermediate: mechanism and rate law

In the case of the second (absorbance-decreasing) reaction stage, the following mechanism can be proposed:

$$W^{V}O_3^- + H^+ \overset{K_{11}}{\leftrightarrows} HW^{V}O_3 \tag{27}$$

$$W^{V}O_3^- + H_2O_2 \overset{K_{12}}{\leftrightarrows} [W^{V}O_2(O_2)]^- + H_2O \tag{28}$$

$$HW^{V}O_3 + H_2O_2 \overset{K_{13}}{\leftrightarrows} H[W^{V}O_2(O_2)] + H_2O \tag{29}$$

$$[W^{V}O_2(O_2)]^- \overset{K_{14}}{\leftrightarrows} [W^{IV}O_2 + O_2^{\bullet -}]_{sc} \tag{30}$$

$$H[W^{V}O_2(O_2)] \overset{K_{15}}{\Longleftrightarrow} [W^{IV}O_2 + HO_2^{\bullet}]_{sc} \tag{31}$$

$$[W^{IV}O_2 + O_2^{\bullet -}]_{sc} \xrightarrow[\text{slow}]{k_{16}} W^{IV}O_2 + O_2^{\bullet -} \tag{32}$$

$$[W^{IV}O_2 + HO_2^{\bullet}]_{sc} \xrightarrow[\text{slow}]{k_{17}} W^{IV}O_2 + HO_2^{\bullet} \tag{33}$$

$$W^{IV}O_2 + H_2O \longrightarrow W^{IV}O^{2+} + 2HO^- \tag{34}$$

We have proposed as the first step of this part of the mechanism the protonation of the long-lived intermediate W(V) in Eq. 27, and that both the non-protonated (Eq. 28) and protonated (Eq. 29) forms of that intermediate react with hydrogen peroxide to yield peroxotungstate(V) complexes. The structure proposed for the non-protonated form of that complex is shown in Scheme 1S, and it can be compared with that of peroxotungstate(VI) ion.

An internal electron transfer from the peroxo ligand to the tungsten(V) atom leads to the formation of either a W(IV)-superoxide radical couple (Eq. 30) or a W(IV)-protonated superoxide radical couple (Eq. 31), both of them again enclosed in a solvent cage, so that when they scape from those solvent cages in the rate-determining steps (Eqs. 32 and 33), and after a posterior hydrolysis (Eq. 34), we have already the main reaction product oxotungsten(IV) ion. Actually, many complexes of oxotungsten(IV) with different ligands are known [77, 78]. A dismutation of the protonated and non-protonated superoxide radicals (as in Eq. 15) will lead to the formation of the other reaction product, diatomic oxygen. The finding that in some experiments the absorbance-decreasing stretch corresponding to the decay of the long-lived intermediate was followed by an

absorbance-increasing one (Fig. 1, right) might indicate that, under some experimental conditions, a further reduction from W(IV) to W(III) took place.

By application of the quasi-equilibrium (to the fast reversible steps given in Eqs. (27–31) and steady state [to the very reactive tungsten(IV) intermediate involved in Eqs. 33 and 34] approximations, we obtain:

$$\frac{d[\mathrm{W(IV)}]}{dt} = (K_{12}K_{14}k_{16} + K_{11}K_{13}K_{15}k_{17}[\mathrm{H^+}])g \tag{35}$$

In this equation:

$$g = \frac{[\mathrm{W(V)}]_\mathrm{T}\,[\mathrm{H_2O_2}]}{1+K_{11}\,[\mathrm{H^+}]} \tag{36}$$

Equations 35 and 36 can explain the results found for the decay of the long-lived intermediate: first order in both tungstate ion and hydrogen peroxide, as well as catalysis by hydrogen ion. Actually, what they predict is a kinetic order 1 for that intermediate. However, it can be experimentally confirmed that the concentration of W(V) at the maximum of the absorbance-time plots for the kinetic runs done in the presence of NaOH is directly proportional to the initial concentration of W(VI). The dependence on the concentration of hydrogen ion is also coherent with the experimental behavior found for this reaction stage (Eq. 6) with:

$$k_{\mathrm{H},4} = K_{12}\,K_{14}\,k_{16}\,[\mathrm{W(V)}]_\mathrm{T}\,[\mathrm{H_2O_2}] \tag{37}$$

$$k_{\mathrm{H},5} = K_{11}K_{13}K_{15}k_{17}[\mathrm{W(V)}]_\mathrm{T}[\mathrm{H_2O_2}] \tag{38}$$

$$k_{\mathrm{H},6} = K_{11} \tag{39}$$

Moreover, the rate decreasing effect of the medium ionic strength for this reaction stage when KCl was used as background electrolyte is consistent with the proposal of a reaction between two unlike charged ions (Eq. 27), so that an increase of the ionic strength is foreseen to result in a weakening of its attractive interaction and a decrease of equilibrium constant K_{11}. On the other hand, the inhibition by phosphate ions experimentally observed indicates that a relatively stable W(V)-phosphate complex might be formed, thus decreasing the rate of decay of the long-lived intermediate.

Finally, the finding of catalysis by transition metal ions [either copper(II), zinc or manganese(II) ions] can be explained in a similar way to that done in relation to the first reaction stage: those ions may act as efficient scavengers for the superoxide radicals (either in their free or protonated forms) locked with the intermediate W(IV) in a solvent cage (Eqs. 30 and 31), hence facilitating the formation of the oxotungsten(IV) ion thought to be the main reaction product (Eq. 34).

Numerical simulations

Some calculations have been done, using the fourth order Runge–Kutta algorithm [69] to perform an approximate integration point by point, keeping free as fitting parameters three molar absorption coefficients (for tungsten species in the forms of reactant, long-lived intermediate and reaction product) and two rate constants (for the formation of the long-lived intermediate and for its decay). When the intermediate formation was assumed to be of second order in W(VI) and its decay of first order, excellent concordances between experimental and theoretical absorbances (deviations affecting the fourth significant figure) were obtained.

Conclusions

By means of a spectrophotometric technique and choosing the wavelength of 225 nm, it has been possible to study two different reaction stages of the tungstate ion-hydrogen peroxide reaction: the formation of a long-lived intermediate at high pH values and its decay at low ones. The formation of the intermediate had an apparent kinetic order for tungstate ion intermediary between one and two, and it was of first order in hydrogen peroxide, whereas the intermediate decay was of first order in both reactants. Both reaction stages showed acid catalysis, as well as catalysis by transition metal ions. The first reaction stage was accelerated by potassium chloride, whereas the second was inhibited by that salt and by phosphate ions. The activation energy of the first stage was unusually close to zero (1.0 ± 1.2 kJ mol^{-1}), but the activation energy of the second stage was considerably higher (28 ± 3 kJ mol^{-1}). A mechanism coherent with the available experimental information has been proposed for the first reaction stage, leading from W(VI) to W(V), and for the second, leading from W(V) to W(IV), an outstanding feature of these mechanisms being the important role played by the solvent cage effect.

Supplementary Information The online version contains supplementary material available at https://doi.org/10.1007/s11144-024-02713-y.

References

1. Cotton FA, Wilkinson G, Murillo CA, Bochmann M (1999) Advanced inorganic chemistry. Wiley, New York
2. Tomiyasu T (1997) Kinetic-mechanistic study of the chlorpromazine-hydrogen peroxide reaction catalyzed by molybdenum(VI) and tungsten(VI), and their differential determination. Anal Chim Acta 349:43–52
3. Zoroddu MA, Medici S, Peana M, Nurchi VM, Lachowicz JI, Laulicht-Glick F, Costa M (2018) Tugnsten or wolfram: friend or foe? Curr Med Chem 25:65–74
4. King DW, Farlow R (2000) Role of carbonate speciation on the oxidation of Fe(II) by H_2O_2. Mar Chem 70:201–209
5. Kaczorowska K, Kolarska Z, Mitka K, Kowalski P (2005) Oxidation of sulfides to sulfoxides. Part 2: oxidation by hydrogen peroxide. Tetrahedron 61:8315–8327

6. Schmitz G (2010) Iodine oxidation by hydrogen peroxide in acidic solutions, Bray–Liebhafsky reaction and other related reactions. Phys Chem Chem Phys 12:6605–6615
7. Yuan FY, Yan JL, Yu W, Du JY, Yu JF (2020) Nitric oxide reduction by hydrogen peroxide absorption through a ceramic hollow fiber membrane contactor. J Environ Chem Eng 8:104129
8. Xu K, Von Gunten U (2021) Permanganate reduction by hydrogen peroxide: formation of reactive manganese species and superoxide and enhanced micropollutant abatement. Sustain Chem Eng 1:1410–1419
9. Gossuin Y, Duez P, Blankert B, Masson C, Laurent S, Rousseau C (2023) Nuclear magnetic resonance relaxometry to monitor chromiun(VI) reduction by hydrogen peroxide, ascorbic acid, and aluminum powder. Magn Reson Chem 61:284–295
10. Perez-Benito JF (2004) Reaction pathways in the decomposition of hydrogen peroxide catalyzed by copper(II). J Inorg Biochem 98:430–438
11. Li HG, Münchberg U, Oughli AA, Buesen D, Lubitz W, Freier E, Plumere N (2020) Suppressing hydrogen peroxide generation to achieve oxygen-insensitivity of a [NiFe] hydrogenase in redox active films. Nat Commun 11:920
12. Yang Y, Ye YH, Shen RQ (2024) Structure and microchannel catalytic bed performance of silver thin films prepared by electroplating. Catalysts 14:39
13. Rukavina-Mikusic A, Rey M, Arean JSA, Vanasco V, Alvarez S, Valdez LB (2023) Mitochondrial H_2O_2 metabolism as central event of heart complex I syndrome in early diabetes. Free Radic Biol Med 201:66–75
14. Zhang W, Zhang L, Yao H, Wang Y, Zhang X, Shang L, Chen X, Zeng J (2023) Long-chain dicarboxylic acids play a critical role in inducing peroxisomal β-oxidation and hepatic triacylglycerol accumulation. J Biol Chem 299:105174
15. Chalifoux O, Faerman B, Mailloux RJ (2023) Mitochondrial hydrogen peroxide production by pyruvate dehydrogenase and α-ketoglutarate dehydrogenase in oxidative eustress and oxidative distress. J Biol Chem 299:105399
16. Perez-Benito JF (2006) A Kinetic study of the cytochrome c-hydrogen peroxide reaction. Collect Czech Chem Commun 71:1588–1610
17. Maksimchuk NV, Puiggali-Jou J, Zalomaeva OV, Larionov KP, Evtushok VY, Soshnikov IE, Sole-Daura A, Kholdeeva OA, Poblet JM, Carbo JJ (2023) Resolving the mechanism for H_2O_2 decomposition over Zr(IV)-substituted lindqvist tungstate: evidence of singlet oxygen intermediacy. ACS Catal 13:10324–10339
18. Ullah N, Guziejewski D, Barton B, Mirceski V (2023) Electrocatalytic reduction of hydrogen peroxide in solution in the presence of polyacrylic acid and copper ions: application for gaseous hydrogen peroxide detection. J Electroanal Chem 951:117918
19. Perez-Benito JF, Marques-Fumado K (2023) Oxidation of hexacyanoferrate(II) ion by hydrogen peroxide: catalysis by molybdate ion. React Kinet Mech Cat 136:2409–2427
20. Weike Z, Yang B (2024) Fabrication of magnetic $MnFe_2O_4$@HL composites with an in situ Fenton-like reaction for enhancing tetracycline degradation. J Colloid Interf Sci 658:997–1008
21. Yong XY, Ji YX, Yang QW, Cheng XL, Zhou J, Zhang XY (2024) Fe-doped g-C_3N_4 with duel active sites for ultrafast degradation of organic pollutants via visible-light-driven photo-Fenton reaction: insight into the performance, kinetics, and mechanism. Chemosphere 351:141135
22. Lin YF, Kotakeyama Y, Li J, Pan YJ, Matsuura A, Ohya Y, Yoshida M, Xiang L, Qi JH (2019) Cucurbitacin B exerts antiaging effects in yeast by regulating autophagy and oxidative stress. Oxid Med Cell Longev 4517091:1–15. https://doi.org/10.1155/2019/4517091
23. Lemoine M (2021) The evolution of the hallmarks of aging. Front Genet 12:693071
24. Mumtaz S, Ali S, Tahir HM, Kazmi SAR, Shakir HA, Mughal TA, Mumtaz S, Summer M, Farook MA (2024) Aging and its treatment with vitamin C: a comprehensive mechanistic review. Mol Biol Rep 48:8141–8153
25. Suh YA, Arnold RS, Lassegue B, Shi J, Xu XX, Sorescu D, Chung AB, Griending KK, Lambeth JD (1999) Cell transformation by the superoxide-generating oxidase Mox1. Nature 401:79–82
26. Gerald D, Berra E, Frapart YM, Chan DA, Giacca AJ, Mansuy D, Pouyssegur J, Yaniv M, Mechta-Grigoriou F (2004) JunD reduces tumor angiogenesis by protecting cells from oxidative stress. Cell 118:781–794
27. Liu J, Li SM, Tang YJ, Cao JL, Hou WS, Wang AQ, Wang C, Jin CH (2024) Jaceosidin induces apoptosis and inhibits migration in AGS gastric cancer cells by regulating ROS-mediated signaling pathways. Redox Rep 29:2313366

28. Pinilla I, Maneu V (2022) Oxidative stress as a main contributor of retinal degenerative diseases. Antioxidants 11:1190
29. Jo HH, Goh YS, Kim HJ, Kim DH, Kim H, Hwang J, Jung JS, Kang NY, Park SE, Park KM, Lee HJ (2023) Tacrolimus improves therapeutic efficacy of umbilical cord blood-derived mesenchymal stem cells in diabetic retinopathy by suppressing DRP1-mediated mitochondrial fission. Antioxidants 12:1727
30. Gyonn-Lee H, Hur J, Won JP, Geuk-Seo H (2024) Ginseng (*Panax ginseng*) leaf extract modulates the expression of heme oxygenase-1 to attenuate osteoclast differentiation. Fitoterapia 173:105831
31. Lemberg R, Foulkes EC (1948) Reaction between catalase and hydrogen peroxide. Nature 161:131–132
32. Quin X, Wu C, Niu DC, Quin LM, Wang X, Wang QG, Li YS (2021) Peroxisome inspired hybrid enzyme nanogels for chemodynamic and photodynamic therapy. Nat Commun 12:5243
33. Shao JX, Cao SP, Che HL, De Mertino MT, Wu HL, Abdelmohsen LKEA, Van Hest JCM (2022) Twin-engine Janus supramolecular nanomotors with counterbalanced motion. J Am Chem Soc 144:11246–11252
34. Georgiou G, Masip L (2003) An overoxidation journey with a return ticket. Science 300:592–594
35. Mohammedi K, Patente TA, Bellili-Muñoz N, Fumeron F, Roussel R, Hadjadj S, Correa-Giannella ML, Marre M, Velho G (2016) Glutathione peroxidase-1 gene (GPX1) variants, oxidative stress and risk of kidney complications in people with type 1 diabetes. Metabolism 65:12–19
36. Zeida A, Trujillo M, Ferrer-Sueta G, Denicola A, Estrin DA, Radi R (2019) Catalysis of peroxide reduction by fast reacting protein thiols. Chem Rev 119:10829–10855
37. Perez-Benito JF, Arias C (1997) A kinetic study of the chromium(VI)-hydrogen peroxide reaction. Role of the diperoxochromate(VI) intermediates. J Phys Chem A 101:4726–4733
38. Scott SH, Bakac A, Espenson JH (1991) Preparation and reactivity of the aquachromium(IV) ion. J Am Chem Soc 113:7787–7788
39. Perez-Benito JF (2006) Formation of superoxochromium(III) by a novel mechanism. Transit Met Chem 31:447–458
40. Al-Ajlouni AM, Espenson JH, Bakac A (1993) Reaction of hydrogen peroxide with the oxochromium(IV) ion by hydride transfer. Inorg Chem 32:3162–3165
41. Perez-Benito JF (2017) Some considerations on the fundamentals of chemical kinetics: steady state, quasi-equilibrium, and transition state theory. J Chem Educ 94:1238–1246
42. Wilkinson F (1980) Chemical kinetics and reaction mechanisms. Van Nostrand Reinhold, New York
43. Li CF, Mizuno N, Yamaguchi K, Suzuki K (2019) Self-assembly of anionic polyoxometalate-organic architectures based on lacunary phosphomolybdates and pyridyl ligands. J Am Chem Soc 141:7687–7692
44. He JY, Bi HX, Liu YQ, Guo MS, An WT, Ma YY, Han ZG (2023) Bridging component strategy in phosphomolybdate-based sensors for electrochemical determination of trace Cr(VI). Inorg Chem 63:842–851
45. Wu L, Li Y, Hua X, Ye L, Yuan C, Liu Z, Zhang HL, Shao X (2024) Radical cation salts of hetera-buckybowls: polar crystals, negative thermal expansion and phase transition. Angew Chem Int Ed Eng 63:202319587
46. Wee LH, Wiktor C, Turner S, Vanderlinden W, Janssens N, Bajpe SR, Houthoofd K, Van Tendeloo G, De Feyter S, Kirschhock CEA, Martens JA (2012) Copper benzene tricarboxylate metal-organic framework with wide permanent mesopores stabilized by Keggin polyoxometallate ions. J Am Chem Soc 134:10911–10919
47. Patel A, Sadasivan R, Patel J (2021) Chiral phosphotungstate functionalized with (S)-1-phenylethylamine: synthesis, characterization, and asymmetric epoxidation of styrene. Inorg Chem 60:10979–10989
48. Zhang YJ, Yang DZ, Yang YL (2024) Cu- and Fe-containing phosphotungstate nanoparticles with POD-like and GSH-like activities to target inhibition of gram-negative bacteria. ACS Appl Nano Mater 7:3950–3959
49. Lafon-Cazal M, Pietri S, Culcasi M, Bockaert J (1993) NMDA-dependent superoxide production and neurotoxicity. Nature 364:535–537
50. Okado-Matsumoto A, Fridovich I (2001) Subcellular distribution of superoxide dismutases (SOD) in rat liver: Cu Zn-SOD in mitochondria. J Biol Chem 276:38388–38393

51. Vance CK, Miller AF (1998) Simple proposal that can explain the inactivity of metal-substituted superoxide dismutases. J Am Chem Soc 120:461–467
52. Ashur I, Brandis A, Greenwald M, Vakrat-Haglili Y, Rosenbach-Belkin V, Scheer H, Scherz A (2003) Control of redox transitions and oxygen species binding in Mn centers by biologically significant ligands: model studies with [Mn]-bacteriochlorophyll a. J Am Chem Soc 125:8852–8861
53. Aguirre JD, Clark HM, McIlvin M, Vazquez C, Palmere SL, Grab DJ, Seshu J, Hart PJ, Saito M, Culotta VC (2013) A manganese-rich environment supports superoxide dismutase activity in a Lyme disease pathogen. Borrelia burgdorferi J Biol Chem 288:8468–8478
54. Perez-Benito JF, Arias C (1999) Mutual catalyst inhibition in the chromium(VI)-copper(II)-hydrogen peroxide reacting system. New J Chem 23:945–949
55. Nagababu E, Rifkind JM (2000) Reaction of hydrogen peroxide with ferrylhemoglobin: superoxide production and heme degradation. Biochemistry 39:12503–12511
56. Alvarez B, Radi R (2001) Peroxynitrite decay in the presence of hydrogen peroxide, mannitol and ethanol: a reappraisal. Free Radic Res 34:467–475
57. Perez-Benito JF, Brillas E, Pouplana R (1989) Identification of a soluble form of colloidal managanese(IV). Inorg Chem 28:390–392
58. Arzamaskova LN, Romanenko AV, Yermakov YI (1980) Kinetics of alkane oxidation by chromic acid in aqueous solutions of Ir(IV) chloride complexes. React Kinet Catal Lett 13:395–400
59. Sellers RM, Simic MG (1976) Pulse radiolysis study of the reactions of some reduced metal ions with molecular oxygen in aqueous solution. J Am Chem Soc 98:6145–6150
60. Scott SH, Bakac A, Espenson JH (1992) Oxidation of alcohols, aldehydes, and carboxylates by the aquachromium(IV) ion. J Am Chem Soc 114:4205–4213
61. Funahashi S, Uchida F, Tanaka M (1978) Reactions of hydrogen-peroxide with metal-complexes. 3. Thermodynamic and kinetics studies on formation, dissociation, and decomposition of peroxochromium(VI) complexes in acid media. Inorg Chem 17:2784–2789
62. El Shahawi MS, Barakat SA (1995) Spectral and electrochemical studies of D-tartaric and DL-mandelic acids with different chromium ions. Spectrochim Acta A 51:171–175
63. Boruah JJ, Ahmed K, Das S, Gogoi SR, Saikia G, Sharma M, Islam NS (2016) Peroxomolybdate supported on water soluble polymers as efficient catalysts for green and selective sulfoxidation in aqueous medium. J Mol Catal A 425:21–30
64. Paul SS, Selim M, Mukherjea KK (2017) Synthesis, characterization and DNA nuclease activity of oxo-peroxomolybdenum(VI) complexes. J Coord Chem 70:1739–1760
65. Babaei B, Bezaatpour A, Basharnavaz H (2020) Robust and fast oxidation of sulfides by immobilized Mo(VI) complex on magnetic nanoparticles in solvent-free condition. Polyhedron 179:114382
66. De la Fuente N, Chen LF, Wang JA, Gonzalez J, Navarrete J (2021) Roles of oxygen defects and surface acidity of Keggin-type phosphotungstic acid dispersed on SBA-15 catalysts in the oxidation of 4,6-dimethyldibenzothiophene. React Kinet Mech Catal 132:1119–1135
67. Zhang ZH, He T, Qi Y, Dai YX, Lao KJ, Gou XC (2022) Rapid and highly specific detection of site-specific 5-hydroxymethylcytosine based on peroxotungstate oxidation and mismatch ligation-based LAMP. RSC Adv 12:19885–19889
68. Herk L, Feld M, Szwarc M (1961) Studies of "cage" reactions. J Am Chem Soc 83:2998–3005
69. Espenson JH (1995) Chemical kinetics and reaction mechanisms. McGraw-Hill, New York
70. Maeda H, Nakamura S, Furuyama T, Segi M (2023) Regioselective rearrangement reactions of naphthylmethyl ethers by using Lewis acid or UV light irradiation. J Mol Struct 1274:134450
71. Sawyer DT, Valentine JS (1981) How super is superoxide? Acc Chem Res 14:393–400
72. Nekovar P, Schrotterova D (2000) Extraction of V(V), Mo(VI) and W(VI) polynuclear species by primene JMT. Chem Eng J 79:229–233
73. Xia XB, Guan WJ, Zhang GQ, Zhou Q, Li QG, Cao ZY, Zheng L, Wu SX (2023) Formation and stability of molybdenum and tungsten species in peroxy solution. J Solut Chem 52:551–569
74. Gumerova NI, Rompel A (2020) Polyoxometalates in solution: speciation under spotlight. Chem Soc Rev 49:7568–7601
75. Inoue H, Hirobe M (1986) Superoxide-dismutase mimetic activity of cytokinin-copper(II) complexes. Biochem Biophys Res Commun 137:372–377
76. Bard AJ, Parsons R, Jordan J (1985) Standard potentials in aqueous solutions. Dekker, New York
77. Pathania MS, Sheikh HN, Kalsotra BL (2006) Synthesis and characterization of cyano complexes of oxotungsten(IV) with morpholinomethyl urea and related ligands. Russ J Inorg Chem 51:1445–1450

78. Sharma M, Saleem M, Singh B, Sheikh HN, Kalsotra BL (2010) Preparation and characterization of cyano complexes of oxotungsten(IV) with Mannich base ligands. E-J Chem 7:378561